GEOLOGY | THE GEOLOGICAL SOCIETY OF AMERICA®

https://doi.org/10.1130/G45323.1

Manuscript received 26 June 2018
Revised manuscript received 24 September 2018
Manuscript accepted 11 November 2018

Published online 7 December 2018

Volcanic activities triggered or inhibited by resonance of volcanic edifices to large earthquakes

Atsuko Namiki[1,2], Eleonora Rivalta[2], Heiko Woith[2], Timothy Willey[2,3,4], Stefano Parolai[5], and Thomas R. Walter[2]
[1]Graduate School of Integrated Arts and Sciences, Hiroshima University, Higashi Hiroshima 739-8521, Japan
[2]GFZ German Research Centre for Geosciences, 14473 Potsdam, Germany
[3]Geosciences, University of Montana, Missoula, Montana 59812, USA
[4]Earth and Environmental Science, University of Potsdam, 14469 Potsdam, Germany
[5]Istituto Nazionale di Oceanografia e di Geofisica Sperimentale, Borgo Grotta Gigante 42/c, 34010 Sgonico TS, Italy

ABSTRACT

The existence of a causal link between large earthquakes and volcanic unrest is widely accepted. Recent observations have also revealed counterintuitive negative responses of volcanoes to large earthquakes, including decreased gas emissions and subsidence in volcanic areas. In order to explore the mechanisms that could simultaneously explain both the positive and negative responses of volcanic activity to earthquakes, we here focus on the role played by topography. In the laboratory, we shook a volcanic edifice analogue, made of gel, previously injected with a buoyant fluid. We find that shaking triggers rapid migration of the buoyant fluid upward, downward, or laterally, depending on the fluid's buoyancy and storage depth; bubbly fluids stored at shallow depth ascend, while low-buoyancy fluids descend or migrate laterally. The migration of fluids induced by shaking is two orders of magnitude faster than without shaking. Downward or lateral fluid migration may decrease volcanic gas emissions and cause subsidence as a negative response, while upward migration is consistent both with an increase in volcanic activity and immediate unrest (deformation and seismicity) after large earthquakes. The fluid migration is more efficient when the oscillation frequency is close to the resonance frequency of the edifice. The resonance frequency for a 30-km-wide volcanic mountain range, such as those where subsidence was observed, is ~0.07 Hz. Only large earthquakes are able to cause oscillation at such low frequencies.

INTRODUCTION

Large earthquakes have been linked to unrest in volcanic areas. Induced activity includes swarms of earthquakes, ground deformation, migration of magmatic gasses, and excitation of geothermal activity; more rarely, eruptions have followed (e.g., Linde and Sacks, 1998; Manga and Brodsky, 2006; Harris and Ripepe, 2007; Hill and Prejean, 2007; Toda et al., 2011; Fujita et al., 2013; Yukutake et. al., 2013; Brenguier et. al., 2014; Aizawa et. al., 2016; Avouris et. al., 2017; Nishimura, 2017; Sawi and Manga, 2018). Recent studies have reported that after the arrival of surface waves from large earthquakes, volcanic degassing increases in basaltic volcanoes, while it decreases in andesitic volcanoes (Avouris et. al., 2017). Permanent subsidence was observed after the A.D. 2010 M_w 8.8 Maule earthquake in the southern Andes (Chile) in volcanic areas adjacent to the ruptured segment of the subduction (Pritchard et al., 2013). After the 2011 M_w 9.0 Tohoku (Japan) earthquake, increased seismicity of the Hakone volcanic complex, crustal deformation around Mount Fuji, and subsidence of volcanic areas in Tohoku were observed (Fujita et al., 2013; Takada and Fukushima, 2013; Yukutake et al., 2013). These observations suggest that large earthquakes can cause, in addition to volcanic unrest, negative responses and a decrease in volcanic activities.

Both static and dynamic stress changes associated with large earthquakes may trigger volcanic eruptions (e.g., Linde and Sacks, 1998; Manga and Brodsky, 2006; Hill and Prejean, 2007). Static stress changes, which cause long-term volumetric expansion and contraction (e.g., Nostro et al., 1998; Walter and Amelung, 2007), decay rapidly outside the source region and cannot entirely explain the widespread seismicity increases observed after the A.D. 1992 Landers earthquake (California, USA; e.g., Hill et al., 1993) and the Tohoku earthquake (Toda et al., 2011). Dynamic stress changes may explain responses at large distances (e.g., Hill and Prejean, 2007). Several mechanisms have been suggested to explain the triggered volcanic activities; i.e., bubble ascent (Steinberg et al., 1989; Sahagian and Proussevitch, 1992; Pyle and Pyle, 1995), liquefaction (Sumita and Manga, 2008), and sloshing (Namiki et al., 2016). Whether these mechanisms can similarly explain the observed negative responses has yet to be determined.

Here, we focus on topography as a site effect (e.g., Paolucci, 2002). The prominent topography of volcanoes focuses the incoming seismic waves that match the resonance frequency of the volcanic edifice and generate dynamic stresses that may activate volcanoes. Topographic loads induce rotations of the principal stress, focusing the trajectories of propagating dikes, and compress just below the edifices so that ascending magmas stall and accumulate at depth (Dahm, 2000; Muller et al., 2001; Watanabe et al., 2002; Kervyn et al., 2009; Roman and Jaupart, 2014; Pinel et al., 2017). The depth of storage depends on the magma buoyancy and the amount of loading stress (Pinel and Jaupart, 2004). Using analogue experiments, we explore how the focusing of dynamic stress by volcanic edifices affects the stability of stored fluids, and how this may lead to their mobilization.

EXPERIMENTAL METHODS

We built an analogue volcanic edifice by solidifying agar gel in a tank covered with a mountain-range–shaped mold of width W (0.14 m) and variable height H (0.04–0.15 m), producing a two-dimensional triangular prism, as denoted in Figure 1A (and in DR Section 1 and Figures DR1

CITATION: Namiki, A., et al., 2018, Volcanic activities triggered or inhibited by resonance of volcanic edifices to large earthquakes: Geology, v. 47, p. 67–70, https://doi.org/10.1130/G45323.1.

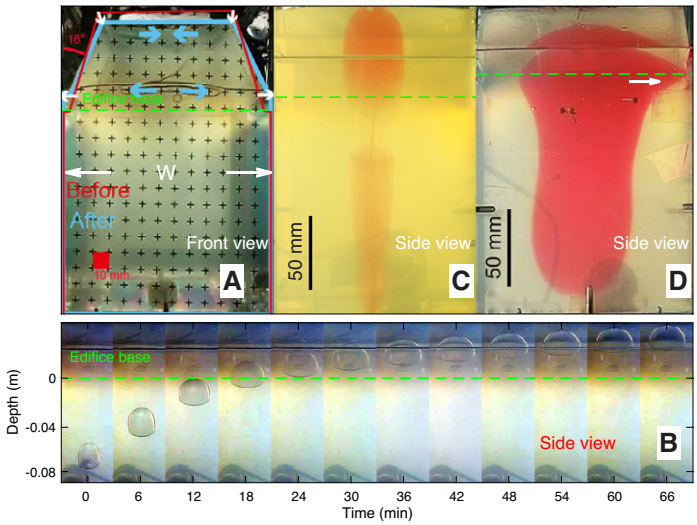

Figure 1. Loading stresses of the experimental gel edifice decelerate the upward propagation of cracks. A: Front view of gel edifice with a width and breadth of *W*. Shape of gel edifice (red frame) readjusts when mold is removed (blue frame) as shown by small white arrows, generating extension (blue arrows) at the base of the edifice (green dashed line). Deviatoric stress field is shown in Figure DR5 (see footnote 1). B: Time lapse of ascending air-filled crack viewed from side. Volume of air in the crack is 1.5 mL and density is 1 kg m^{-3}. Air-filled crack decelerates as it reaches edifice base. The effect of the discontinuous refraction index is removed (Fig. DR6). In this experiment, buoyancy pressure is $\Delta\rho g l \approx 280$ Pa, where $\Delta\rho = 1139$ kg m^{-3} is the density difference between the gel and the fluids filling the cracks, $g = 9.8$ m s^{-2} is gravitational acceleration, and $l = 0.025$ m is vertical length of fluid column. C: Crack trajectory visualized by injection of red-dyed water after ascent shown in B. D: Broader crack generated by injecting red-dyed water reaches the sidewall, as shown by white arrow. Water density is 1000 kg m^{-3} and volume is 15 mL. This results in $\Delta\rho = 140$ kg m^{-3}, $l = 0.2$ m, and $\Delta\rho g l \approx 270$ Pa, similar to that of the air-filled crack shown in B.

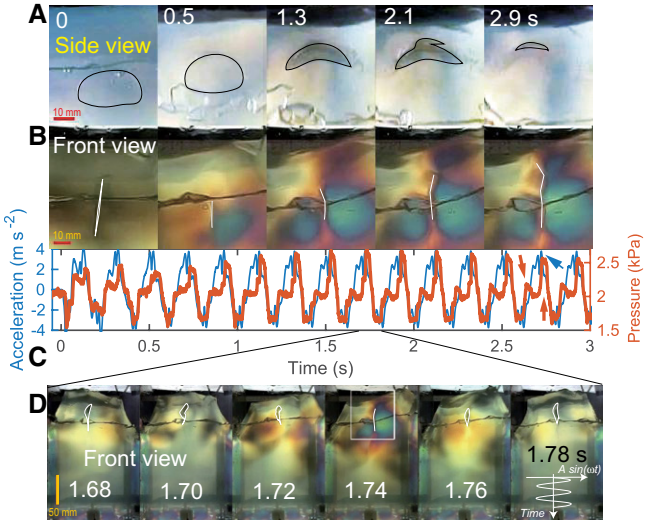

Figure 2. Rapid ascent of air-filled crack upon shaking. The gel edifice, with a fundamental resonance frequency of 3.8 Hz (Table DR1 [see footnote 1]), containing an air-filled crack with volume of 1.5 mL, is shaken laterally with a frequency of 5 Hz and displacement amplitude of $A = 3$ mm. A,B: Side (A) and front (B) views of area shown by white box in D. C: Measured pressure of gel edifice (red curve) and acceleration of shaking table (blue curve) have different numbers of peaks, as denoted by arrows. D: Time evolution of stress field during half-cycle of oscillation. Direction of imposed displacement, $A\sin(\omega t)$ (where A is displacement amplitude, ω is angular frequency, and *t* is time), is denoted in lower right panel. Bluish to reddish colors in B and D are higher to lower stress concentrations, respectively, highlighted by photoelasticity. Locations of air-filled crack in A, and in B and D, are traced by black and white curves, respectively.

and DR2 in the GSA Data Repository[1]). The elastic gel used as a rock analogue (Figs. DR3 and DR4; Table DR1) has a density of ρ = 1134–1144 kg m^{-3} and a shear modulus of $G = 200$–1300 Pa. Its stress perturbations are observable using photoelasticity by placing a polarizing sheet in front of and behind the gel edifice. When we removed the mold, the gel edifice shrank vertically and dilated laterally under its own weight, resulting in horizontal extension at the edifice base (Fig. 1A, yellowish color; Fig. DR5).

To simulate crack propagation, we injected a buoyant fluid (dyed water or air) into the bottom of the gel edifice and observed the deceleration of the ascending fluid-filled cracks induced by the edifice loading (Fig. DR5). Air-filled cracks decelerate and vertically shorten when entering the gel edifice (Figs. 1B and 1C). In contrast, water-filled cracks, which are broader in shape due to their higher density and larger volume required for propagation, reach the sidewall at the base of the gel edifice (white arrow in Fig. 1D; Fig. DR7; Kervyn et al., 2009; Taisne et al., 2011). Then, we shake the edifice-crack system on a shaking table using various values of displacement amplitude A and angular frequency ω (Fig. 2; Fig. DR1).

EXPERIMENTAL RESULTS AND DISCUSSION

When we shook the gel edifice at 5 Hz with an air-filled crack at its base (Fig. 2A; Movie DR1 in the Data Repository), it took only 3 s for the crack to ascend to the top of the edifice, as opposed to 30 min without shaking. A large stress concentration accumulated around the crack (bluish region in Figs. 2B and 2D; 1.74 s). Because the slopes of the edifice reflect the elastic waves, the imposed and reflected waves interfere. The maximum stress at the crack tip enhanced by the wave interference was larger than that before the shaking, and was close to the yield threshold. As a result, the fracture accelerated (Figs. DR3, DR5, DR8, and DR9). Air flowed quickly into the newly fractured crack tip, leading to a prompt eruption (DR Section 2).

The wave interference was also observed in the pressure curve measured at the bottom of the tank (Fig. 2C; Fig. DR1). Initially (<0.5 s), the pressure waveform closely followed that of the imposed acceleration, but after some time (>1.5 s) the pressure peak split into two. The wave interference arose twice in each oscillation cycle; it first appeared as the small peak, and then the overlap of the interference and the shaking cycle appeared as the large peak (red arrows in Fig. 2C).

When shaking the gel edifice at 5 Hz with a red-dyed water-filled crack at the edifice base, the crack propagated both upward and laterally (Fig. 3; Movies DR2 and DR3). Dynamic stresses cause a rotation of the principal stresses and variations of amplitude over time, which changed the direction of the crack propagation intermittently, resulting in a zigzag pathway highlighted by the red-dyed water (white arrows in Fig. 3; 9 s). Fluid-filled cracks propagate perpendicular to the maximum tensile direction, in general (Anderson, 1951). Unlike the air-filled crack, the water-filled crack spread horizontally at the edifice base. After we resumed shaking at 8 Hz, the crack immediately reached the sidewall (green arrow in Fig. 3A; 15 s). Without shaking, a similar water-filled crack took more than 30 min to migrate over the same distance (Fig. 1D). When a mixture of air and liquid was injected (Fig. DR10; Movie DR4), air bubbles accumulated at the crack tip; upon shaking, the bubbles moved upward while some part of the liquid descended.

The force acting on an oscillating edifice with mass M during shaking equals $MA\omega^2$. Dividing this force by W^2, which is the area of the edifice base, gives the stress $\sigma_b = MA\omega^2/W^2$ (DR Section 3). Dividing σ_b by G, we obtain the strain $\gamma = MA\omega^2/(GW^2)$. Given that stress $\sigma_b = MA\omega^2/W^2 \propto H$, taller edifices are affected by larger stresses during shaking. We here do

[1]GSA Data Repository item 2019027, methods, additional results, Tables DR1 and DR2, Figures DR1–DR15, and Movies DR1–DR5, is available online at http://www.geosociety.org/datarepository/2019/, or on request from editing@geosociety.org.

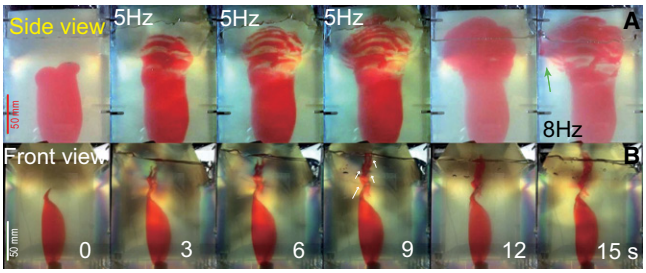

Figure 3. Accelerated ascent of water-filled crack upon shaking, shown from side (A) and front (B) views. Crack makes a zigzag pathway (white arrows in B) and reaches the sidewall (green arrow in A).Crack has volume of 25 mL and buoyancy pressure of 150 < Δρ*gl* < 270 Pa (where Δρ is the density difference between the gel and the fluids filling the cracks, *g* is gravitational acceleration, and *l* is vertical length of fluid column). The gel edifice, with a fundamental resonance frequency of 4.2 Hz, is shaken with 3 mm amplitude at 5 Hz from 0 to 10 s, and at 8 Hz from 14 to 15 s; i.e., no shaking between 10 and 14 s.

not consider edifice bending, observed in our gel edifices with low shear modulus but not realistic in nature. Most cracks propagated when $\gamma \approx 1$ (Fig. DR11C), which is the yield condition of our gel (Fig. DR3C). Some cracks propagated for $\gamma < 1$ and some failed to propagate for $\gamma > 1$, suggesting that additional requirements exist for crack propagation.

The stress σ_b is amplified through interference if the oscillation period of the incident wave is equal to the travel time across the width of the edifice, which is W/v_s (where v_s is the shear wave velocity), and $v_s = 0.4$–1.1 m s^{-1} in our experiments. The inverse of this travel time, v_s/W, is close to the resonance frequency of small-aspect-ratio edifices, i.e., with $H/W < 0.5$ (Figs. DR8 and DR12; Table DR1; DR Section 4; Paolucci, 2002; Towhata, 2008).

The fluid-filled cracks propagated more efficiently when the imposed shaking frequency was close to the fundamental resonance frequency of the gel edifice (Fig. 4A). Higher modes of the resonance frequencies (normalized by the fundamental resonance frequency ~2) also promoted crack propagation. At the highest frequency (normalized frequency >5), crack propagation became less likely, suggesting that fluid migration is difficult under a rapidly changing stress field (DR Section 5).

COMPARISON WITH NATURAL VOLCANOES

Our experimental arrangement differs from natural conditions in several aspects. The aspect ratios of our gel edifices are in the range of 0.28–1.1, larger than typical values for isolated volcanoes (0.05–0.3; Kervyn et al., 2009) and for the volcanic mountain ranges where subsidence was observed after earthquakes (0.03, Fig. DR13). Buttressing of the rigid walls in our experiments likely affected the resonance of the edifice and interference of elastic waves. Under natural conditions, the largest displacement of an edifice base may be caused by Rayleigh waves in a vertical direction, different from the horizontal shaking in our experiments.

We thus numerically simulated horizontal and vertical oscillations of a volcanic edifice with an aspect ratio of 0.03, situated on a homogeneous layer of 15 km thickness, similar to the thickness of the upper crust (Fig. DR14; DR Section 6). The simulations show that both horizontal and vertical oscillations result in stress focusing and amplification of the displacement beneath the edifice where magmas may accumulate (Fig. DR14; Movie DR5). Therefore, we consider resonance of natural volcanic edifices plausible.

Natural volcanoes have a more complex shape and internal structure than our gel edifice, so we expect that they resonate over a range of frequencies. This may cause fluid migration and redistribution in more complex ways than those we observed in our experiments.

The low shear modulus of our gel exaggerates strains in ways that are unrealistic in rock. This is a limit common to many experiments using a gel as an analogue for rock. However, our experiments are well-scaled regarding stress balance. That is, in Table DR2, we compare stresses of σ_b, $\Delta\rho gl$ (l is the vertical length of the fluid column), and fracture pressure P_F, and find that their ratios in our experiments and in natural volcanoes are similar. We also find that σ_b in nature may be similar to or larger than the stress changes estimated to trigger volcanic unrest (DR Section 3). Our gel attenuates waves more efficiently than rock, suggesting that amplification by resonance may be more efficient in nature. A difference in attenuation does not affect the resonance frequency.

IMPLICATIONS FOR SUBSIDENCE AND GAS EMISSION CHANGES

Finally, we applied our experiments to triggered negative responses of volcanic activity to large earthquakes. The fundamental resonance frequency of volcanic mountain ranges with aspect ratios of $H/W < 0.5$ is ~$0.7 \times v_s/W$ (Paolucci, 2002). Assuming $v_s = 3$ km s^{-1} for the shallow crust, the resonance frequency of the volcanic mountain range in Tohoku, Japan, with a width of ~30 km (Fig. DR13), becomes 0.07 Hz. Seismic waves recorded after the Tohoku earthquake close to the subsidence area in Iwate, Tohoku, show a frequency peak at ~0.07 Hz (Fig. DR15), suggesting that resonance did occur.

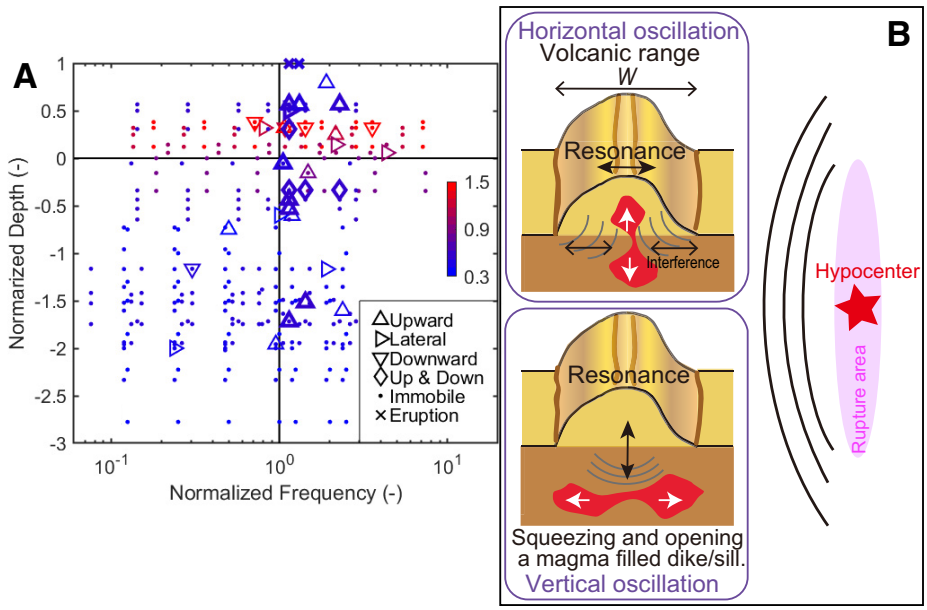

Figure 4. Response of fluid to shaking. A: Direction of fluid migration (see legend) upon shaking, mapped as a function of imposed frequency normalized by the fundamental resonance frequency of the gel edifice (Table DR1 [see footnote 1]), and the depth of the crack tip at onset of shaking, normalized by the edifice height. Crosses indicate that the crack reaches the edifice summit. Symbols with thick outlines indicate that fluid in the crack is air (as a liquid-free fluid) or bubbly fluids. Symbol color indicates aspect ratio of edifice, as denoted in the color bar; reddish colors indicate taller edifices. Crack propagation depends on imposed frequency, edifice loading, buoyancy of the internal fluid, and the stress field deviated by the resonance at the base of edifice (see details in Fig. DR11). B: Schematic illustration of positional relationship between the source region of a large earthquake and the resonating volcanic mountain range with a width of *W*. Interference of elastic waves from the volcano slopes pushes out magma from the chamber.

The permanent subsidence associated with the Tohoku earthquake could be a result of static stress change (Pritchard et al., 2013; Takada and Fukushima, 2013). However, the observed stress orientation did not change. In terms of the differential stress, it is not clear whether static stress change caused new crack openings (Toda et al., 2011; Yoshida et al., 2012).

Resonance of volcanoes and volcanic mountain ranges to shaking may be consistent with the diversity of observed responses to earthquakes, including both positive and negative responses. Vertical oscillation of volcanoes may push out the fluids in magmatic or hydrothermal reservoirs, or in the groundwater system beneath the volcano (Fig. 4B), redistributing fluids and potentially causing subsidence (Pritchard et al., 2013; Takada and Fukushima, 2013). This may also explain the observed drop in seismic-wave velocities after the Tohoku earthquake (Brenguier et al., 2014).

Different responses observed at volcanoes of different composition (Avouris et al., 2017) can be explained by magma migration induced by resonance, by taking into account the viscosity dependence of bubble separation efficiency. Only if the viscosity of the surrounding melt is low enough, can bubbles separate from the melt upon shaking, to increase the outgassing (Namiki et al., 2016).

In conclusion, in our experiments, resonance of the gel edifice causes stress enhancement around fluid-filled cracks, promoting crack propagation and accelerating fluid migration. Similarly, our estimates suggest that resonance of a volcano, induced by large earthquakes, can promote redistribution of magma or other fluids in the volcano, triggering or inhibiting volcanic activity.

ACKNOWLEDGMENTS

We thank D.P. Hill, Tohru Watanabe, five anonymous reviewers, and editor Mark Quigley for comments and reviews; Naoki Uchida for helpful discussion of the seismic data analysis; and Ralf Bauz, Stefan Mikulla, Peter Neuendorf, and Yukie Tanaka for their help in the laboratory. This work was supported by a Japan Society for the Promotion of Science (JSPS) Grant-in-Aid for Scientific Research (KAKENHI 17H05316), the JSPS–DAAD Researcher Exchange Program, and the Mitsubishi Foundation research grant 27132.

REFERENCES CITED

Aizawa, K., et al., 2016, Gas pathways and remotely triggered earthquakes beneath Mount Fuji, Japan: Geology, v. 44, p. 127–130, https://doi.org/10.1130/G37313.1.

Anderson, E.M., 1951, The Dynamics of Faulting and Dyke Formation with Applications to Britain: Edinburgh, Oliver and Boyd, 206 p.

Avouris, D.M., Carn, S.A., and Waite, G.P., 2017, Triggering of volcanic degassing by large earthquakes: Geology, v. 45, p. 715–718, https://doi.org/10.1130/G39074.1.

Brenguier, F., Campillo, M., Takeda, T., Aoki, Y., Shapiro, N.M., Briand, X., Emoto, K., and Miyake, H., 2014, Mapping pressurized volcanic fluids from induced crustal seismic velocity drops: Science, v. 345, p. 80–82, https://doi.org/10.1126/science.1254073.

Dahm, T., 2000, On the shape and velocity of fluid-filled fractures in the Earth: Geophysical Journal International, v. 142, p. 181–192, https://doi.org/10.1046/j.1365-246x.2000.00148.x.

Fujita, E., Kozono, T., Ueda, H., Kohno, Y., Yoshioka, S., Toda, N., Kikuchi, A., and Ida, Y., 2013, Stress field change around the Mount Fuji volcano magma system caused by the Tohoku megathrust earthquake, Japan: Bulletin of Volcanology, v. 75, 679, https://doi.org/10.1007/s00445-012-0679-9.

Harris, A.J.L., and Ripepe, M., 2007, Regional earthquake as a trigger for enhanced volcanic activity: Evidence from MODIS thermal data: Geophysical Research Letters, v. 34, L02304, https://doi.org/10.1029/2006GL028251.

Hill, D.P., and Prejean, S.G., 2007, Dynamic triggering, *in* Kanamori, H., ed., Treatise on Geophysics, Volume 4: Earthquake Seismology: Amsterdam, Elsevier, p. 257–291, https://doi.org/10.1016/B978-044452748-6.00070-5.

Hill, D.P., et al., 1993, Seismicity remotely triggered by the magnitude 7.3 Landers, California, earthquake: Science, v. 260, p. 1617–1623, https://doi.org/10.1126/science.260.5114.1617.

Kervyn, M., Ernst, G.G.J., van Wyk de Vries, B., Mathieu, L., and Jacobs, P., 2009, Volcano load control on dyke propagation and vent distribution: Insights from analogue modeling: Journal of Geophysical Research, v. 114, B03401, https://doi.org/10.1029/2008JB005653.

Linde, A.T., and Sacks, I.S., 1998, Triggering of volcanic eruptions: Nature, v. 395, p. 888–890, https://doi.org/10.1038/27650.

Manga, M., and Brodsky, E., 2006, Seismic triggering of eruptions in the far field: Volcanoes and geysers: Annual Review of Earth and Planetary Sciences, v. 34, p. 263–291, https://doi.org/10.1146/annurev.earth.34.031405.125125.

Muller, J.R., Ito, G., and Martel, S.J., 2001, Effects of volcano loading on dike propagation in an elastic half-space: Journal of Geophysical Research, v. 106, p. 11,101–11,113, https://doi.org/10.1029/2000JB900461.

Namiki, A., Rivalta, E., Woith, H., and Walter, T.R., 2016, Sloshing of a bubbly magma reservoir as a mechanism of triggered eruptions: Journal of Volcanology and Geothermal Research, v. 320, p. 156–171, https://doi.org/10.1016/j.jvolgeores.2016.03.010.

Nishimura, T., 2017, Triggering of volcanic eruptions by large earthquakes: Geophysical Research Letters, v. 44, p. 7750–7756, https://doi.org/10.1002/2017GL074579.

Nostro, C., Stein, R.S., Cocco, M., Belardinelli, M.E., and Marzocchi, W., 1998, Two-way coupling between Vesuvius eruptions and southern Apennine earthquakes, Italy, by elastic stress transfer: Journal of Geophysical Research, v. 103, p. 24,487–24,504, https://doi.org/10.1029/98JB00902.

Paolucci, R., 2002, Amplification of earthquake ground motion by steep topographic irregularities: Earthquake Engineering & Structural Dynamics, v. 31, p. 1831–1853, https://doi.org/10.1002/eqe.192.

Pinel, V., and Jaupart, C., 2004, Magma storage and horizontal dyke injection beneath a volcanic edifice: Earth and Planetary Science Letters, v. 221, p. 245–262, https://doi.org/10.1016/S0012-821X(04)00076-7.

Pinel, V., Carrara, A., Maccaferri, F., Rivalta, E., and Corbi, F., 2017, A two-step model for dynamical dike propagation in two dimensions: Application to the July 2001 Etna eruption: Journal of Geophysical Research: Solid Earth, v. 122, p. 1107–1125, https://doi.org/10.1002/2016JB013630.

Pritchard, M.E., Jay, J.A., Aron, F., Henderson, S.T., and Lara, L.E., 2013, Subsidence at southern Andes volcanoes induced by the 2010 Maule, Chile earthquake: Nature Geoscience, v. 6, p. 632–636, https://doi.org/10.1038/ngeo1855.

Pyle, D.M., and Pyle, D.L., 1995, Bubble migration and the initiation of volcanic eruptions: Journal of Volcanology and Geothermal Research, v. 67, p. 227–232, https://doi.org/10.1016/0377-0273(94)00111-S.

Roman, A., and Jaupart, C., 2014, The impact of a volcanic edifice on intrusive and eruptive activity: Earth and Planetary Science Letters, v. 408, p. 1–8, https://doi.org/10.1016/j.epsl.2014.09.016.

Sahagian, D.L., and Proussevitch, A.A., 1992, Bubbles in volcanic systems: Nature, v. 359, p. 485, https://doi.org/10.1038/359485a0.

Sawi, T.M., and Manga, M., 2018, Revisiting short-term earthquake triggered volcanism: Bulletin of Volcanology, v. 80, 57, https://doi.org/10.1007/s00445-018-1232-2.

Steinberg, G.S., Steinberg, A.S., and Merzhanov, A.G., 1989, Fluid mechanism of pressure growth in volcanic (magmatic) systems: Modern Geology, v. 13, p. 257–265.

Sumita, I., and Manga, M., 2008, Suspension rheology under oscillatory shear and its geophysical implications: Earth and Planetary Science Letters, v. 269, p. 468–477, https://doi.org/10.1016/j.epsl.2008.02.043.

Taisne, B., Tait, S., and Jaupart, C., 2011, Conditions for the arrest of a vertical propagating dyke: Bulletin of Volcanology, v. 73, p. 191–204, https://doi.org/10.1007/s00445-010-0440-1.

Takada, Y., and Fukushima, Y., 2013, Volcanic subsidence triggered by the 2011 Tohoku earthquake in Japan: Nature Geoscience, v. 6, p. 637–641, https://doi.org/10.1038/ngeo1857.

Toda, S., Stein, R.S., and Lin, J., 2011, Widespread seismicity excitation throughout central Japan following the 2011 M=9.0 Tohoku earthquake and its interpretation by Coulomb stress transfer: Geophysical Research Letters, v. 38, L00G03, https://doi.org/10.1029/2011GL047834.

Towhata, I., 2008, Geotechnical Earthquake Engineering: Berlin, Springer-Verlag, 684 p., https://doi.org/10.1007/978-3-540-35783-4.

Walter, T.R., and Amelung, F., 2007, Volcanic eruptions following M ≥ 9 megathrust earthquakes: Implications for the Sumatra-Andaman volcanoes: Geology, v. 35, p. 539–542, https://doi.org/10.1130/G23429A.1.

Watanabe, T., Masuyama, T., Nagaoka, K., and Tahara, T., 2002, Analog experiments on magma-filled cracks: Competition between external stresses and internal pressure: Earth, Planets, and Space, v. 54, p. e1247–e1261, https://doi.org/10.1186/BF03352453.

Yoshida, K., Hasegawa, A., Okada, T., Iinuma, T., Ito, Y., and Asano, Y., 2012, Stress before and after the 2011 great Tohoku-oki earthquake and induced earthquakes in inland areas of eastern Japan: Geophysical Research Letters, v. 39, L03302, https://doi.org/10.1029/2011GL049729.

Yukutake, Y., Miyazawa, M., Honda, R., Harada, M., Ito, H., Sakaue, M., Koketsu, K., and Yoshida, A., 2013, Remotely triggered seismic activity in Hakone volcano during and after the passage of surface waves from the 2011 M9.0 Tohoku-Oki earthquake: Earth and Planetary Science Letters, v. 373, p. 205–216, https://doi.org/10.1016/j.epsl.2013.05.004.

Printed in USA